Article:

He, T orcid.org/0000-0001-8975-8667, Zhu, M, Mills, BJW orcid.org/0000-0002-9141-0931 et al. (7 more authors) (2019) Possible links between extreme oxygen perturbations and the Cambrian radiation of animals. Nature Geoscience, 12 (6). pp. 468-474. ISSN 1752-0894

https://doi.org/10.1038/s41561-019-0357-z

Supplementary information for

Possible links between extreme oxygen perturbations and the Cambrian radiation of animals

Tianchen He*, Maoyan Zhu, Benjamin J.W. Mills, Peter M. Wynn, Andrey Yu. Zhuravlev, Rosalie Tostevin, Philip A. E. Pogge von Strandmann, Aihua Yang, Simon W. Poulton, Graham A. Shields

*Correspondence and requests for materials should be addressed to T.H. (T.He@leeds.ac.uk)

SI Guide:

Supplementary Notes

Supplementary Figs. S1 to S7

Supplementary Tables S1 and S2

Captions for Supplementary Tables S3 to S5

Supplementary References

Additional supplementary files (separate files):

Supplementary Table S3 (Excel file)

Supplementary Table S4 (Excel file)

Supplementary Table S5 (Excel file)

Supplementary Notes:

Geology, stratigraphic, lithological, palaeontological context, and samples. The type sections of the lower Cambrian subdivisions and their lower boundaries are located in the south-eastern part of the Siberian Platform. The main sections are outcrop along the Aldan and Lena rivers (Supplementary Fig. S1) and are suggested to have formed in a normal-salinity, shallow, open marine environment[1]. Samples were collected from seven lower Cambrian carbonate-dominated sections along the Aldan and Lena rivers, and in ascending Siberian Stage stratigraphic order include Dvortsy, Isit', Zhurinsky Mys, Ulakhan-Kyyry-Taas, Ulakhan-Tuoidakh, Labaia and Tit-Ary sections. These sections are the stratotype sections for the lower Cambrian chronostratigraphic units used in Russia, and the total thickness of the sequences is ~600 m, spanning the Cambrian Stage 2 to Stage 4 interval. Importantly, the GSSPs of the Cambrian stages 2–4 are not determined, but the provisional international subdivision is largely based on the fossil distribution and stages established in these Siberian sections. Moreover, since the Aldan-Lena rivers sections are unique with respect to archaeocyath, trilobite, and other fossils abundances, and many of these forms were found from all over the world, these subdivisions are globally recognised. The investigated sedimentological sequence is represented mainly by micritic/sparitic limestones with well-preserved skeletal (exclusively benthic), ooid, marine cement fabrics[2–6] and only a few dolomitic beds. Nearly 400 well-preserved carbonate samples were systematically collected following the regional stratigraphic guidebook for the lower Cambrian subdivision of the Siberian Platform[1], with a sampling resolution of roughly 50 cm to 1 m spacing. 352 well-preserved carbonates were analysed for carbon and oxygen isotopes; 142 samples were analysed for carbonate-associated sulphate (CAS) sulphur isotopes, concentrations of diagenetic-diagnostic elements, and [CAS].

Age model. Carbon isotope results shown in Supplementary Table S3 and Fig. 1 confirm the long-term $\delta^{13}C$ trend, values and amplitudes of all short-term carbon-isotope oscillations presented in previous studies on the Siberian Platform[4,7,8]. The current study recovered three full carbonate $\delta^{13}C_{carb}$ positive excursions (III, VI, VII), the rising limb of IV and the falling limb of V. These sections are finely subdivided by both archaeocyath and trilobite zones which are globally correlated. An age model consistent with the internationally agreed numerical time scale[9] is applied to the studied sections. The stratigraphically calibrated age for the base of Series 2 (= base Stage 3) was suggested to be ~521 Ma[9], and is the age tie point for the FAD of trilobites (base of the *Profallotaspis jakutensis* Trilobite Zone and of the Atdabanian Stage) on the Siberian Platform. This estimate derives largely from a radiometrically determined age of 520.93±0.4 Ma, which can be tied to the basal part of positive carbon isotope excursion IV in Morocco[10,11] and Siberian Aldan-Lena rivers sections (Fig. 1). A volcanic ash bed in Shropshire, England yields an U–Pb zircon age for the middle *Callavia* Trilobite Zone of 514.45±0.36 Ma[12] and provides an estimate for the age of the uppermost Atdabanian *Fansycyathus lermontovae* Archaeocyath Zone on the Siberian Platform[11,13]. The well-known early Cambrian Konservat-Lagerstätte – South China Chengjiang biota (Maotianshan Shale Member, Yu'anshan Formation) – is correlated with the interval from the *Delgadella anabara* Zone to lower *Judomia* Zone in Siberia[9]. The Chengjiang biota is assigned an age of ~516–517 Ma based on the age model in the current study, which is consistent with the recently reported numerical age, based on detrital zircon U–Pb analyses, which constrain the Chengjiang biota to no older than 518.03 Ma[14]. Accordingly, the Sirius Passet Lagerstätte is correlated with the Laurentian *Esmeraldina rowei* Trilobite Zone, approximately corresponding to the upper *Judomia* Trilobite Zone in Siberia[15] and assigned an age of ~514.5–515 Ma in the current age model. In addition, U–Pb zircon analyses for the middle *Callavia* Trilobite Zone constrain the age of the basal Botoman (Stage 4) *Bergeroniellus micmacciformis* – *Erbiella* Trilobite Zone to be 514 Ma. Ash beds of 511±1.0 Ma and 509.1±0.22 Ma occur in strata bearing fossils from the *Geyerorodes howleyi* and *Acadoparadaxides harlani* trilobite zones of the former Avalon continent, which encompasses eastern Newfoundland, the southern British Isles and some other areas[12,16], and thus brackets the Toyonian/Amgan (Series 2/3) boundary in Siberia at ~510 Ma[17]. A constant sediment accumulation rate (0.007 Myr/m) is assumed between the *Lermontovia grandis* Trilobite Zone, which is time equivalent with the *Geyerorodes howleyi* Zone (~511 Ma), and the lowermost Botoman *Bergeroniellus micmacciformis – Erbiella Zone* (514.45 Ma) in Fig. 1 based on current and previously reported stratigraphic thickness in between[4]. Based on the calculation, an age of ~512 Ma is suggested for the topmost stratigraphic horizon (middle *Bergeroniellus ketemensis* Zone) as shown in Fig. 1. Therefore, three age tie points including 512 Ma, 514.45 Ma, and 521 Ma are applied to the studied stratigraphy (Supplementary Table S3 and Fig. 1). The age assignment for each sample assumes constant sediment accumulation rates between age tie points. The full age framework and its correlation with archaeocyath, trilobite, and small shelly fossil biozones are shown in Supplementary Table S3.

Source of biodiversity data. The Alden-Lena Rivers carbonate platform represents a unique setting for the preservation of early Cambrian marine animal biodiversity – of the c. 2000 recorded early Cambrian genera, 350 were described for the first time at this site, and over half of all known global biodiversity is represented on this platform[1,13,18]. Biodiversity data have been collated at the species level (e.g. beta-diversity of reefal palaeocommunities) for the Siberian platform and at the genus level globally[4,6,13]. A new part of this compilation and basic sources are reported in Zhuravlev and Wood (2018), omitting synonyms and poorly identified forms[19]. The majority of these biodiversity data were obtained from the same reference sections as samples for C- and S-isotope analyses in the current study. Data collected from other sections can be clearly correlated to the Aldan-Lena Rivers sections through visual tracing of individual lithological beds within the Siberian platform. Indeed, the beta-diversity data for reefal palaeocommunities were obtained from the exact same reference section[20].

Evaluating diagenesis. It is important to constrain the degree to which bulk carbonate or skeletal components (both low-Mg calcite) have been altered to establish whether geochemical trends are likely to be representative of syndepositional oceanic values. Interaction with diagenetic fluids (e.g. meteoric, burial fluids) during dissolution and recrystallisation of shallow marine carbonates can simultaneously lower the $\delta^{13}C$ and $\delta^{18}O$ values in carbonate rocks[21–24]. Therefore, a positive correlation between $\delta^{13}C$ and $\delta^{18}O$ is often considered to be a tentative indicator of diagenetic alteration. As shown in Supplementary Fig. S5, $\delta^{13}C$ v. $\delta^{18}O$ cross-plots for the Aldan-Lena river sections exhibit only weak positive correlation (R^2 = 0.213). Although this trends to support only minor diagenetic overprinting, we note that non-diagenetic covariations can arise even in seemingly primary trends, such as in the long-term Ordovician $\delta^{13}C$ and $\delta^{18}O$ record[25]. More convincingly, the $\delta^{13}C$ records shown in Fig. 1 exhibit a gradual and extremely smooth curve through Cambrian stages 2-4, and both the long-term trends and magnitudes of short-term $\delta^{13}C$ excursions are globally identical[9,26], which is a robust indication of its primary nature. Furthermore, previous study of materials at Siberian Aldan-Lena rivers sections also shows that $\delta^{13}C$ values exhibit isotopic consistency between skeletal fabrics, primary marine cement and micrite analysed from the same carbonate rock[4]. Therefore, $\delta^{13}C$ and $\delta^{18}O$ systematics of the Aldan-Lena rivers sections are likely to represent primary isotopic signatures of coeval seawater rather than alteration during diagenesis.

Carbonate associated sulphate (CAS), whereby marine sulfate is structurally substituted into the carbonate lattice, is considered to be a robust proxy archive that records syndepositional seawater sulphate, if CAS $\delta^{34}S$ values and concentration have not been impacted by diagenetic overprinting[27–29]. Previous work has shown that CAS content decreases in carbonates as they undergo exchange with burial fluids at increasing degrees of burial depth and temperature[29–31]. Despite changes in CAS concentrations, no significant variations in the CAS sulphur isotopic composition were found during progressive burial diagenesis[29,32]. These results suggest that CAS $\delta^{34}S$ values are resistant to late stage burial alteration, but analysed CAS concentration from a bulk carbonate may not be considered a reliable indicator of original seawater sulphate levels. CAS contents in this study are consistently high (majority > 100 ppm), and exhibit no correlation with $\delta^{34}S$ ($R^2 = 0.025$) (Supplementary Fig. S5). Post-depositional dolomitisation also has the potential to influence $\delta^{34}S$ values of CAS[33] and simultaneously alter carbonate $\delta^{18}O$ values[34], but dolomitic samples were avoided during sampling, and no correlation is seen between $\delta^{34}S$ values and Mg/Ca ($R^2 = 0.003$) or $\delta^{18}O$ ($R^2 = 0.008$) (Supplementary Fig. S5), indicating that $\delta^{34}S$ values do not vary due to partial dolomitisation.

Early diagenetic exchange with pore fluids can also produce changes in the isotopic composition and abundance of CAS. For example, sulphate reduction in anoxic pore waters causes progressive enrichment of ^{34}S in the residual sulphate pool, in tandem with a decline in sulfate concentrations. During carbonate burial, if neomorphism of primary aragonitic phases to calcite occurs in a critical interval where sulphate is abundant, but also isotopically enriched, CAS may be altered towards elevated $\delta^{34}S$[31,35]. Variability in CAS $\delta^{34}S$ values may be present between different sedimentary components in bulk carbonate rocks[36]. Our samples show no obvious evidence for recrystallisation from an earlier aragonitic phase, but do include a mixture of calcified fossils with micritic and sparitic textures in a few samples from the interval with coupled $\delta^{13}C$-$\delta^{34}S$ cycles (Supplementary Fig. S7). However, no correlations are observed between $\delta^{34}S$ values and HCl-leachable carbonate content (R^2 = 0.002) or Mg/Ca (R^2 = 0.003) (Supplementary Fig. S5), suggesting that variability in lithology or carbonate phases did not exert a diagenetic control over the variations in CAS $\delta^{34}S$ records. The current $\delta^{34}S$ record may derive from an integrated signal of homogenized bulk rock carbonate associated sulphate that is close to the coeval seawater. Also, cross-plots of CAS $\delta^{34}S$ values show no correlation with traditional indicators of diagenesis, including CAS concentration (R^2 = 0.025), Mn/Sr ($R^2 < 0.0001$) or $\delta^{18}O$ (R^2 = 0.008) (Supplementary Fig. S5), suggesting that the samples could potentially preserve primary seawater sulphate $\delta^{34}S$ values.

CAS may be contaminated by either the oxidation of pyrite or present-day secondary atmospheric sulphate (SAS) during the chemical extraction[33,37]. Our analysed samples are generally low in petrographically visible pyrite (except for carbonates of Sinsk Formation) and precautions were taken to minimise the potential for pyrite oxidation during carbonate acid dissolution (see Methods). Present-day SAS should only be incorporated into the bulk carbonate rock at leachable sites via weathering, and would generally not affect the primary calcite lattices where CAS is located. The current study applied multiple consecutive NaCl pre-leaches, which demonstrate the elimination of soluble sulphate contaminants (see Methods), therefore minimising potential SAS contamination. Finally, the observed $\delta^{34}S$ trend and excursions (Fig. 1) show an extremely smooth curve with minor scatter, likely resulting from variability in primary isotopic signature in the early Cambrian seawater sulphate, rather than variable diagenetic overprinting or experimental contamination.

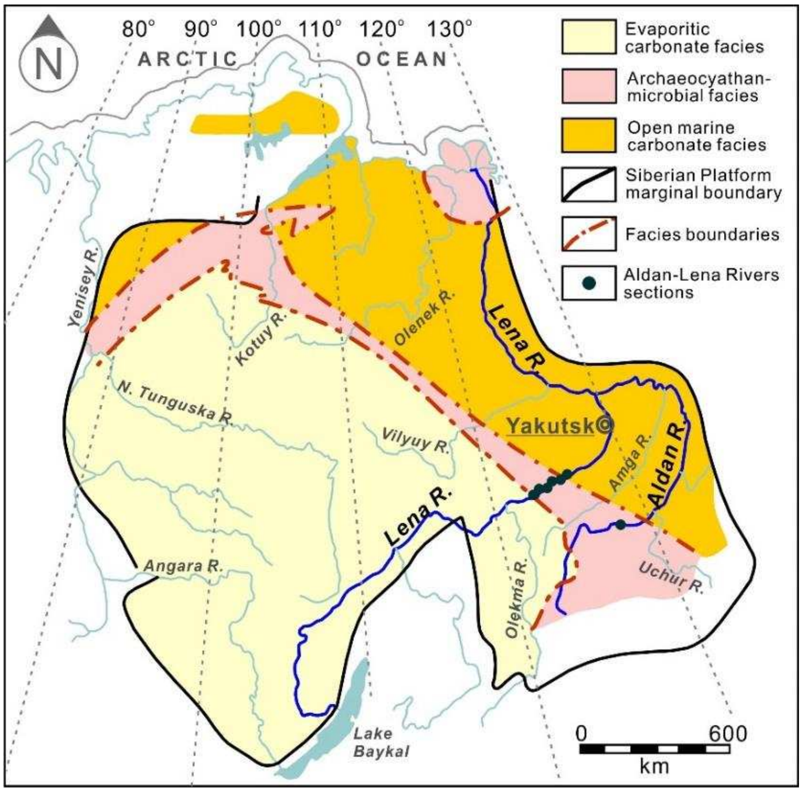

Supplementary Fig. S1. Simplified geological map of the Siberian Platform during the early Cambrian. The map shows modern rivers, major sedimentary facies basins and localities of studied sections. R.: river.

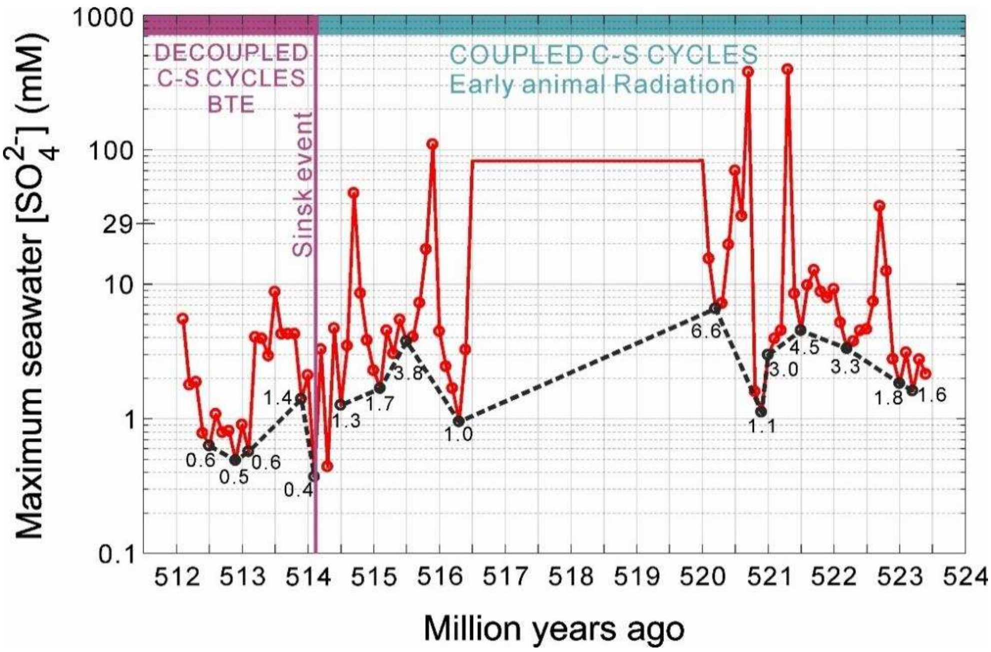

Supplementary Fig. S2. Secular variation of maximum seawater sulphate concentration [SO_4^{2-}] from Cambrian Stage 2 to Stage 4 (~524-512 Ma) for the southeastern Siberian platform. The resulting red curve exhibits variations in maximum seawater [SO_4^{2-}] with data smoothing grids at 0.1 Myr (red). The black dotted line represents the lower end of the data envelope and the best estimate of variation in sulphate concentration. [SO_4^{2-}] values are marked next to the black dotted data points representing the lowest values for the 0.5 Myr bands. Coupled C-S cycles: interval of animal radiation when $\delta^{13}C$ and $\delta^{34}S$ records are positively correlated; Decoupled C-S cycles: interval when $\delta^{13}C$ and $\delta^{34}S$ records are decoupled. BTE: Botoman–Toyonian Extinction.

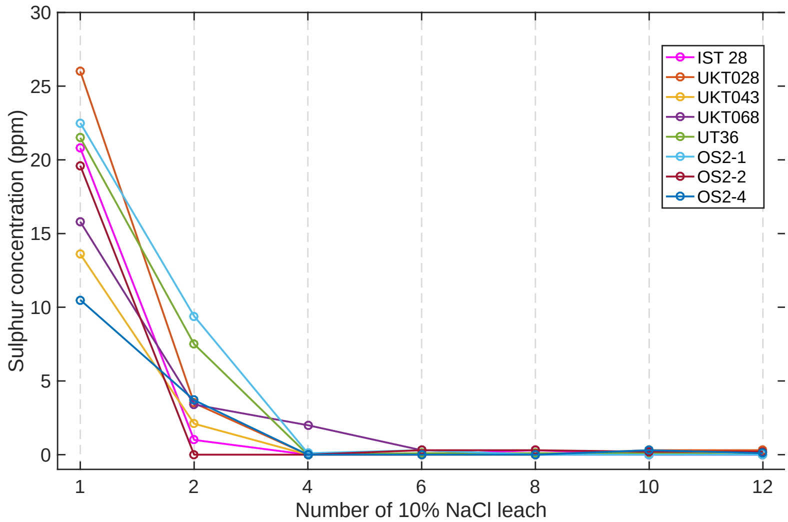

Supplementary Fig. S3. Sulphur concentration variations in 10% sodium chloride-leached solution from different stages of multiple leaching (leach 1, 2, 4, 6, 8, 10, 12). Test samples IST28, UKT028, UKT043, UKT068, UT36 are Cambrian carbonate from the Siberian Aldan-Lena rivers sections. OS2-1, OS2-2, OS2-4 are test samples of marine carbonate from the Ediacaran Nama Group, Namibia.

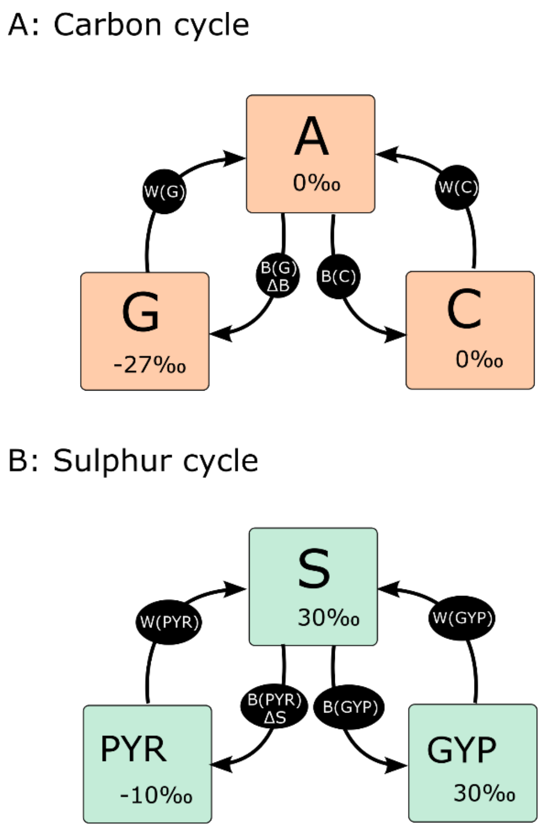

Supplementary Fig. S4. Coupled C-S cycle model diagram. Boxes show reservoirs and arrows show fluxes. Burial fluxes are denoted 'B' and weathering fluxes are denoted 'W'. A denotes atmosphere and ocean carbon, S denotes oceanic sulphate. G is buried organic carbon, C is buried carbonate, PYR is buried pyrite and GYP is buried gypsum. ΔB and ΔS are the fractionation factors associated with the burial of organic carbon (G) and pyrite (PYR) relative to the ocean/atmosphere fractionation. The assumed isotopic composition of reservoirs for the standard model run are shown underneath the reservoir titles.

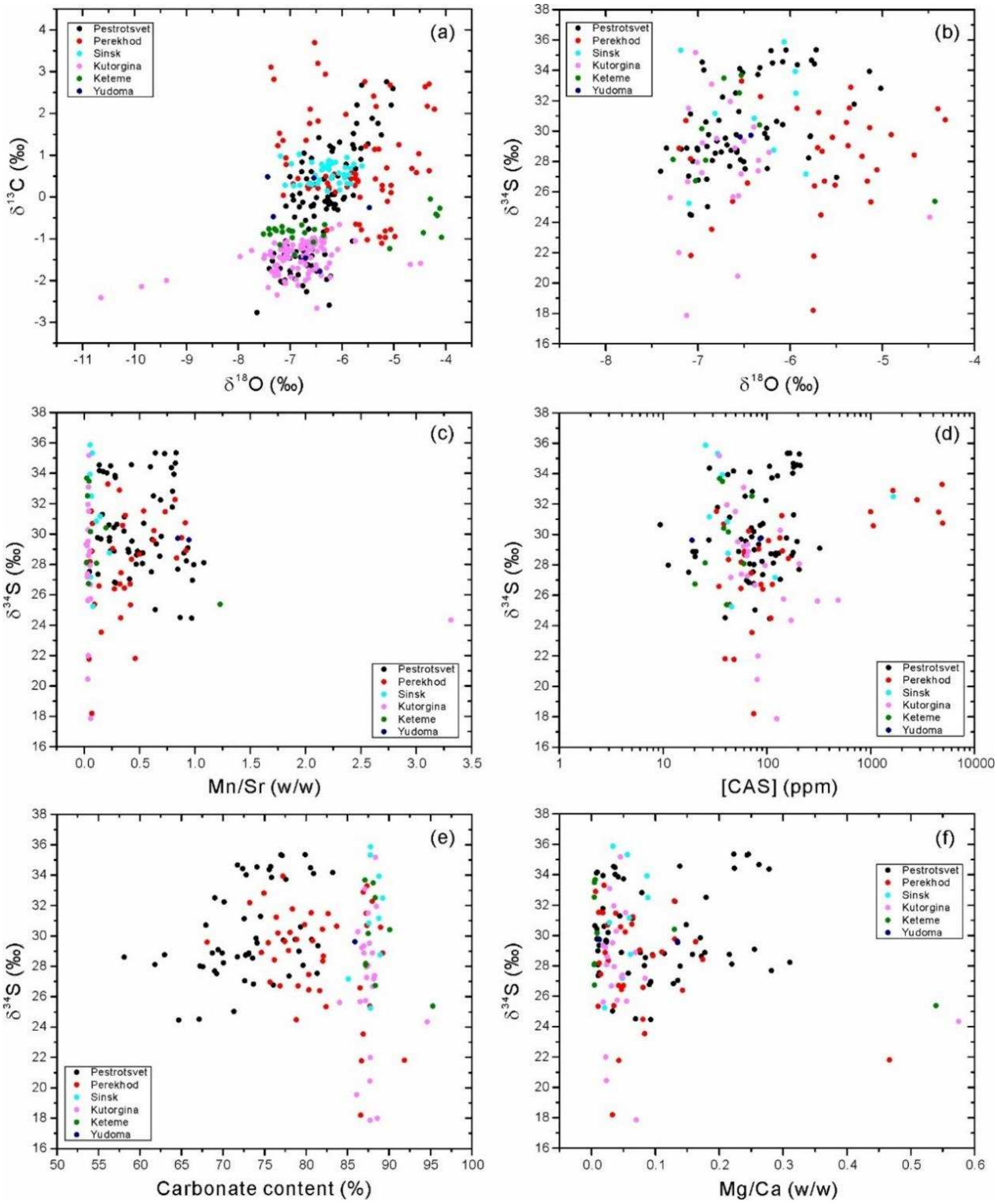

Supplementary Fig. S5. Cross-plots of elemental concentration and isotopic values of carbonates. a. $\delta^{18}O$ (‰)–$\delta^{13}C$ (‰) ($R^2 = 0.213$). **b.** $\delta^{34}S$ (‰)–$\delta^{18}O$ (‰) ($R^2 = 0.008$). **c.** $\delta^{34}S$ (‰)–Mn/Sr (w/w) ($R^2 < 0.0001$). **d.** $\delta^{34}S$ (‰)–[CAS] (ppm) ($R^2 = 0.025$). **e.** $\delta^{34}S$ (‰)–carbonate content (%) ($R^2 = 0.002$). **f.** $\delta^{34}S$ (‰)–Mg/Ca (w/w) ($R^2 = 0.003$). Different colours represent different stratigraphic formations of the Aldan-Lena rivers sections. Carbonate content (%): weight percentages of HCl-leachable $CaCO_3$ and $CaMg(CO_3)_2$ in carbonate samples. No correlation is observed in any of the cross-plots, indicating minimal digenetic alteration to CAS $\delta^{34}S$.

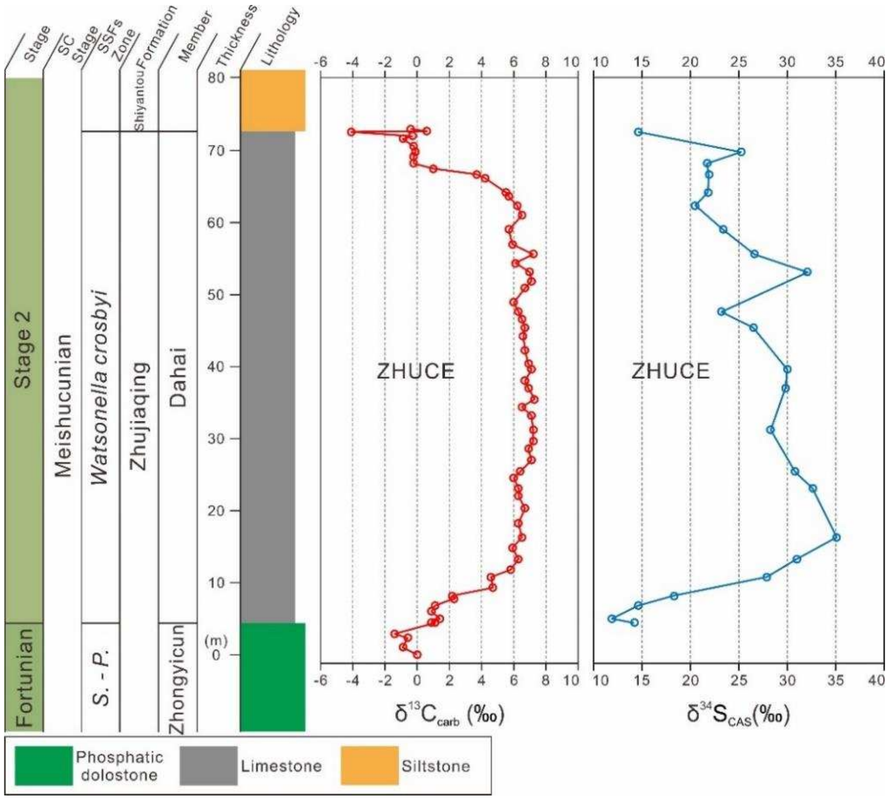

Supplementary Fig. S6. High-resolution carbonate carbon ($\delta^{13}C_{carb}$) and carbonate-associated sulphate sulphur isotope ($\delta^{34}S_{CAS}$) records of early Cambrian Stage 2 to Stage 4 at Xiaotan section, South China. $\delta^{13}C_{carb}$ data are previously published[38]. The regional Stage subdivision is shown next to the global subdivision plan for comparison[38]. SC Stage: South China Stage; Abbreviations: SSFs = small shelly fossils; *S. – P.* = *Siphogonuchites triangularis* – *Paragloborilus subglobosus*. ZHUCE = ZHUjiaqing Carbon isotope Excursion. The early Stage 2 ZHUCE event shows positive covariance between $\delta^{13}C_{carb}$ and $\delta^{34}S_{CAS}$ as observed in the Siberian Aldan-Lena rivers sections of Cambrian Stages 2-3, likely representing the first atmospheric oxygenation pulse in the early Cambrian. The ZHUCE event also coincides a rapid diversification event of small shelly fauna[9,39–41].

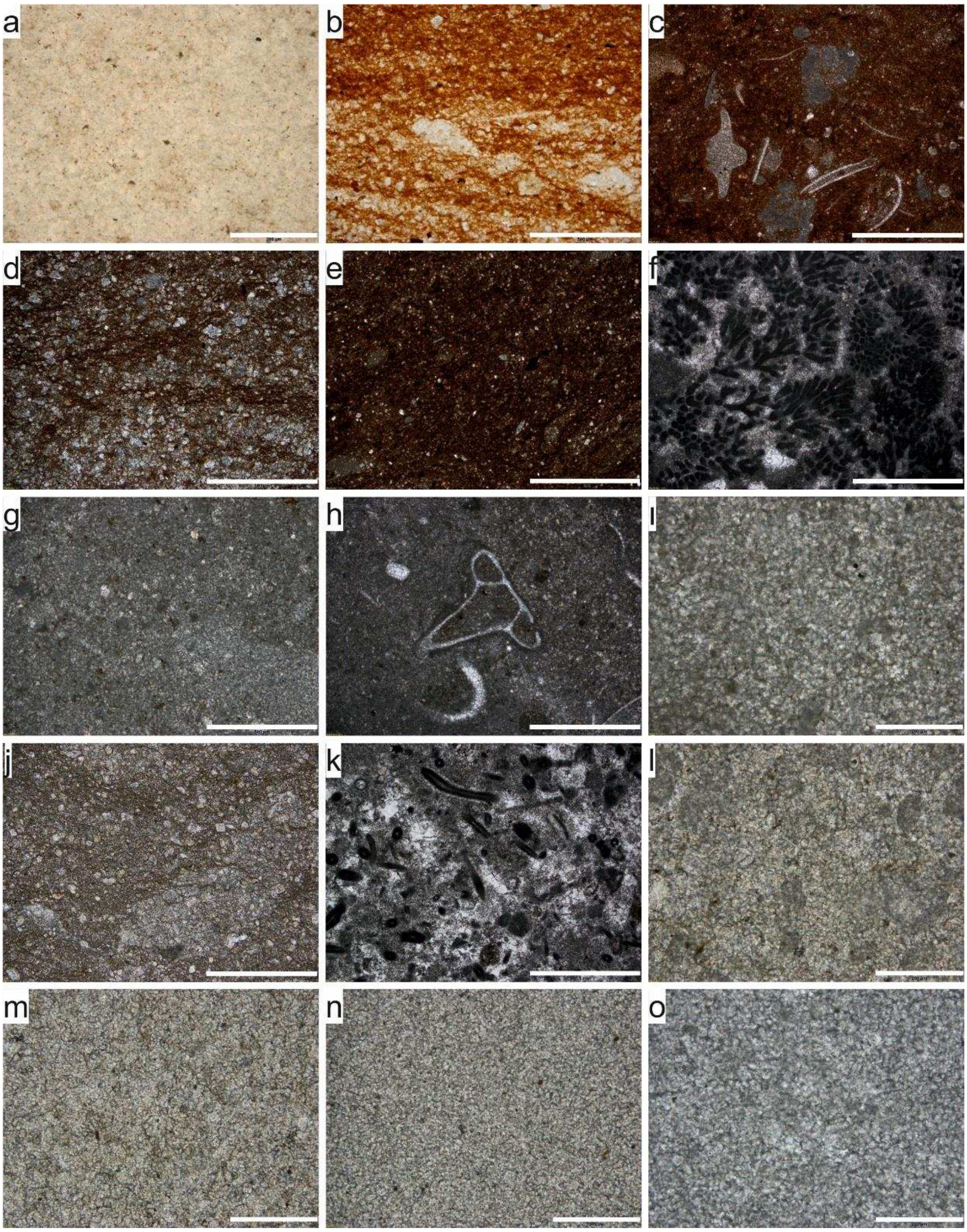

Supplementary Fig. S7. Representative thin-section photomicrograph (plane-polarised light) of carbonate samples used for C-, S-isotope study at Siberian Aldan-Lena rivers sections. (a) micritic sample (IST03, Pestrotsvet Formation, Tommotian Stage) showing fine-grained calcite with minimal siliciclastic content, scale bar = 200 μm. (b) sparitic sample (IST19, Pestrotsvet Formation, Tommotian Stage) with partially recrystallised spars, scale bar = 500 μm. (c) biosparite (IST26, Pestrotsvet Formation, Tommotian Stage) with abundant small shelly fossils (mostly chancelloriids, molluscs and hyoliths) and iron-rich siliciclastic content, scale bar = 1 mm. (d) sparitic sample (IST47, Pestrotsvet Formation, Tommotian Stage) with partially recrystallised spar, scale bar = 500 µm. (e) sparitic sample (ZHU01, Pestrotsvet Formation, Atdabanian Stage) with partially recrystallised spars and iron-rich siliciclastic content, scale bar = 1 mm. (f) micritic carbonate (ZHU09, Pestrotsvet Formation, Atdabanian Stage) with abundant calcimicrobe or microproblematic framework organism, *Gordonophyton*, scale bar = 1 mm. (g-h) microsparite (UKT032, Perekhod Formation, Atdabanian Stage) with the presence of primarily aragonitic chancelloriid *sclerites*, scale bar = 500 µm. (i) coarsely grained dolostone (UKT043, Perekhod Formation, Atdabanian Stage), scale bar = 200 µm. (j) sparitic sample (UKT051, Perekhod Formation, Botoman Stage) with partially recrystallised spars and siliciclastic content, scale bar = 500 µm. (k) biosparitic carbonate (UT03, Perekhod Formation, Botoman Stage) with probable abundant tubular calcimicrobe *Proaulopora*, scale bar = 1 mm. (l) microsparite sample (UKT101, Sinsk Formation, Botoman Stage) contained fine-grained calcite and calcimicrobe fragments, scale bar = 200 µm. (m) microsparite sample (UT27, Sinsk Formation, Botomian) contained fine-grained calcite, scale bar = 200 µm. (n) microsparite sample (LAB56, Kutorgina Formation, Botoman Stage) contained fine-grained calcite, scale bar = 200 µm. (o) microsparite sample (TA28, Keteme Formation, Toyonian Stage) contained fine-grained calcite, scale bar = 200 µm

Isotope excursions/trends	***P***	***R^2***	***RMSE***
III	0.54	0.32	1.64
IV	0.94	0.92	0.96
V	0.60	0.73	1.21
VI	0.64	0.53	1.57
VII	0.74	0.55	2.14
~524–514 Ma	0.50	0.26	2.53
~514–512 Ma	0.076	0.001	4.9

Supplementary Table S1. Statistical correlation parameters for paired short-term $\delta^{13}C$ and $\delta^{34}S$ excursions and long-term trends. The goodness of fit is indicated by the Pearson index, the coefficient of determination (R^2) and root mean square error (*RMSE*). For Pearson (*P*) and R-square (R^2), closer to one indicate a better correlation between C-S isotopic data; For *RMSE*, smaller number indicate better correlation. ~524–514 Ma: interval when $\delta^{13}C$ and $\delta^{34}S$ records are positively correlated at Aldan-Lena Rivers sections; ~514–512 Ma: interval when $\delta^{13}C$ and $\delta^{34}S$ records decoupled.

Flux	Symbol	Rate
Organic C weathering	W(G)	$4 \times 10^{12}\ mol\ yr^{-1}$
Organic C burial	B(G)	Calculated from isotope mass balance
Carbonate weathering	W(C)	$12 \times 10^{12}\ mol\ yr^{-1}$
Carbonate burial	B(C)	$12 \times 10^{12}\ mol\ yr^{-1}$
Pyrite weathering	W(PYR)	$2 \times 10^{12}\ mol\ yr^{-1}$
Pyrite burial	B(PYR)	Calculated from organic C availability
Gypsum weathering	W(GYP)	$1 \times 10^{12}\ mol\ yr^{-1}$
Gypsum burial	B(GYP)	Calculated to maintain a steady state
Parameter	**Symbol**	**Value**
Ocean/atmosphere carbon	A	$3.3 \times 10^{18}\ mol$
Ocean sulphate	S	Varied, present day = $42 \times 10^{18}\ mol$
Isotopic composition of A	δA	Data in this study
Isotopic composition of S	δS	Predicted from model
Isotopic composition of G	δG	Varied, average = $-27‰$
Isotopic composition of C	δC	Varied, average = $0‰$
Isotopic composition of PYR	δPYR	-10
Isotopic composition of GYP	δGYP	30
Fractionation factor: carbon	ΔB	27
Fractionation factor: sulphur	ΔS	40

Supplementary Table S2. List of coupled carbon and sulphur cycle model fluxes and parameters.

Captions for Supplementary Table S3:

Stratigraphic context, age model, litho-, biostratigraphy, sequence stratigraphy and geochemical data for the Aldan-Lena rivers sections. Abbreviations: TA = Tit-Ary; LAB = Labaia; AT = Achchagy-Tuydakh; UT = Ulakhan-Tuoidakh; UKT = Ulakhan-Kyyry-Taas; AKT = Achchagy-Kyyry-Taas; Z Mys and ZHU = Zhurinsky Mys; IST = Isit'; DVO = Dvortsy; SSFs = small shelly fossils; CAS = carbonate-associated sulphate; Carbonate% = total HCl-leachable carbonate content. Siberian Platform sequence stratigraphic data are reconstructed from the Aldan-Lena rivers region[5]. Carbon isotope data numbered as AT, AKT, Z Mys are obtained from the pioneering study[4] to fill the sampling gap in the current study. Sulphur isotope and elemental concentration were obtained from the current study. All elemental analyses represent total 10% HCl-leachable elemental contents of bulk carbonate samples.

Captions for Supplementary Table S4:

Number of total animal species per sampling unit for the Cambrian stages 2-4 at the Siberian Aldan-Lena rivers sections.

Captions for Supplementary Table S5:

Stratigraphic context, litho-, biostratigraphy and C- and S-isotope data for the Xiaotan section, South China. Carbon isotope data are previously published[38]. S-isotope data are from the present study using CAS extraction and isotope analytical protocols described in Methods.

Supplementary References

1. Varlamov, A. I. *et al. The Cambrian System of the Siberian Platform Part 1 : The Aldan-Lena Region*. (PIN RAS, 2008).

2. Astashkin, V. A. *et al*. Cambrian System on the Siberian Platform. Correlation chart and explanatory notes. *Int. Union Geol. Sci. Publ.* 1–133 (1991).

3. Derry, L. A., Brasier, M. D., Corfield, R. M., Rozanov, A. Yu. & Zhuravlev, A. Yu. Sr and C isotopes in Lower Cambrian carbonates from the Siberian craton: A paleoenvironmental record during the 'Cambrian explosion'. *Earth Planet. Sci. Lett.* **128**, 671–681 (1994).

4. Brasier, M. D., Corfield, R. M., Derry, L. A., Rozanov, A. Yu. & Zhuravlev, A. Yu. Multiple $\delta^{13}C$ excursions spanning the Cambrian explosion to the Botomian crisis in Siberia. *Geology* **22**, 455 (1994).

5. Zhuravlev, A. Yu. Outlines of the Siberian platform sequence stratigraphy in the Lower and lower Middle Cambrian (Lena-Aldan area). *Rev. Española Paleontol.* 105–114 (1998).

6. Zhuravlev, A. Yu. & Wood, R. A. Anoxia as the cause of the mid-Early Cambrian (Botomian) extinction event. *Geology* **24**, 311 (1996).

7. Brasier, M. D., Rozanov, A. Yu., Zhuravlev, A. Yu., Corfield, R. M. & Derry, L. A. A carbon isotope reference scale for the Lower Cambrian succession in Siberia: report of IGCP Project 303. *Geol. Mag.* **131**, 767 (1994).

8. Dahl, T. W. *et al.* Reorganisation of Earth's biogeochemical cycles briefly oxygenated the oceans 520 Myr ago. *Geochemical Perspect. Lett.* **3**, 210–220 (2017).

9. Peng, S., Babcock, L. E. & Cooper, R. A. The Cambrian Period. in *The Geologic Time Scale 2012* (eds. Gradstein, F. M., Ogg, J. G., Schmitz, M. D. & Ogg, G. M.) 437–488 (Elsevier Science Limited, 2012).

10. Maloof, A. C. *et al.* Constraints on early Cambrian carbon cycling from the duration of the Nemakit-Daldynian–Tommotian boundary $\delta^{13}C$ shift, Morocco. *Geology* **38**, 623–626 (2010).

11. Zhang, X. *et al.* Challenges in defining the base of Cambrian Series 2 and Stage 3. *Earth-Science Rev.* **172**, 124–139 (2017).

12. Harvey, T. H. P. *et al.* A refined chronology for the Cambrian succession of southern Britain. *J. Geol. Soc. London.* **168**, 705–716 (2011).

13. Zhuravlev, A. Yu. & Riding, R. (eds.) *The ecology of the Cambrian radiation*. (Columbia University Press, 2001).

14. Yang, C., Li, X., Zhu, M., Condon, D. J. & Chen, J. Geochronological constraint on the

Cambrian Chengjiang biota, South China. *J. Geol. Soc. London.* **175**, 659–666 (2018).

15. Hollingsworth, J. S. Lithostratigraphy and biostratigraphy of Cambrian Stage 3 in Western Nevada and Eastern California. *Museum North. Arizona Bull.* 26–42 (2011).

16. Landing, E. *et al.* Duration of the Early Cambrian: U-Pb ages of volcanic ashes from Avalon and Gondwana. *Can. J. Earth Sci.* **35**, 329–338 (1998).

17. Sundberg, F. A. *et al.* International correlation of the Cambrian Series 2-3, Stages 4-5 boundary interval. *Australas. Paleontol. Mem.* **49**, 83–124 (2016).

18. Butorin, A. *et al. Lena Pillars Nature Park. Potential World Heritage Property*. (Natural Heritage Protection Fund, 2012).

19. Zhuravlev, A. Yu. & Wood, R. A. The two phases of the Cambrian Explosion. *Sci. Rep.* **8**, 1–10 (2018).

20. Zhuravlev, A. Yu. & Naimark, E. B. Alpha, beta, or gamma: Numerical view on the Early Cambrian world. *Palaeogeogr. Palaeoclimatol. Palaeoecol.* **220**, 207–225 (2005).

21. Brand, U. & Veizer, J. Chemical diagenesis of a multicomponent carbonate system -2: stable isotopes. *J. Sediment. Res.* **51**, (1981).

22. Banner, J. L. & Hanson, G. N. Calculation of simultaneous isotopic and trace element variations during water-rock interaction with applications to carbonate diagenesis. *Geochim. Cosmochim. Acta* **54**, 3123–3137 (1990).

23. Allan, J. R. & Matthews, R. K. Isotope signatures associated with early meteoric diagenesis. *Sedimentology* **29**, 797–817 (1982).

24. Lu, M. *et al.* The DOUNCE event at the top of the Ediacaran Doushantuo Formation, South China: Broad stratigraphic occurrence and non-diagenetic origin. *Precambrian Res.* **225**, 86–109 (2013).

25. Shields, G. A. *et al.* Sr, C, and O isotope geochemistry of Ordovician brachiopods: a major isotopic event around the Middle-Late Ordovician transition. *Geochim. Cosmochim. Acta* **67**, 2005–2025 (2003).

26. Maloof, A. C. *et al.* The earliest Cambrian record of animals and ocean geochemical change. *Geol. Soc. Am. Bull.* **122**, 1731–1774 (2010).

27. Fike, D. A., Bradley, A. S. & Rose, C. V. Rethinking the Ancient Sulfur Cycle. *Annu. Rev. Earth Planet. Sci.* **43**, 593–622 (2015).

28. Paytan, A. & Gray, E. T. Sulfur Isotope Stratigraphy. in *The Geologic Time Scale* (eds. Gradstein, F. M., Ogg, J. G., Schmitz, M. D. & Ogg, G. M.) 167–180 (Elsevier, 2012).

29. Gill, B. C., Lyons, T. W. & Frank, T. D. Behavior of carbonate-associated sulfate during meteoric diagenesis and implications for the sulfur isotope paleoproxy. *Geochim. Cosmochim. Acta* **72**, 4699–4711 (2008).

30. Staudt, W. J. & Schoonen, M. A. A. Sulfate Incorporation into Sedimentary Carbonates. *Geochemical Transform. Sediment. Sulfur* **612**, 332–345 (1995).

31. Rennie, V. C. F. & Turchyn, A. V. The preservation of $\delta^{34}S_{SO4}$ and $\delta^{18}O_{SO4}$ in carbonate-associated sulfate during marine diagenesis: A 25 Myr test case using marine sediments. *Earth Planet. Sci. Lett.* **395**, 13–23 (2014).

32. Fichtner, V. *et al.* Diagenesis of carbonate associated sulfate. *Chem. Geol.* **463**, 61–75 (2017).

33. Wotte, T., Shields-Zhou, G. A. & Strauss, H. Carbonate-associated sulfate: Experimental comparisons of common extraction methods and recommendations toward a standard analytical protocol. *Chem. Geol.* **326**–**327**, 132–144 (2012).

34. Vasconcelos, C., McKenzie, J. A., Warthmann, R. & Bernasconi, S. M. Calibration of the $\delta^{18}O$ paleothermometer for dolomite precipitated in microbial cultures and natural environments. *Geology* **33**, 317 (2005).

35. Busenberg, E. & Niel Plummer, L. Kinetic and thermodynamic factors controlling the distribution of SO_3^{2-} and Na^+ in calcites and selected aragonites. *Geochim. Cosmochim. Acta* **49**, 713–725 (1985).

36. Present, T. M., Paris, G., Burke, A., Fischer, W. W. & Adkins, J. F. Large Carbonate associated sulfate isotopic variability between brachiopods, micrite, and other sedimentary components in Late Ordovician strata. *Earth Planet. Sci. Lett.* **432**, 187–198 (2015).

37. Peng, Y. *et al.* Widespread contamination of carbonate-associated sulfate by present-day secondary atmospheric sulfate: Evidence from triple oxygen isotopes. *Geology* **42**, 815–818 (2014).

38. Li, D. *et al.* Carbon and strontium isotope evolution of seawater across the Ediacaran–Cambrian transition: Evidence from the Xiaotan section, NE Yunnan, South China. *Precambrian Res.* **225**, 128–147 (2013).

39. Zhu, M.-Y., Babcock, L. E. & Peng, S.-C. Advances in Cambrian stratigraphy and paleontology: Integrating correlation techniques, paleobiology, taphonomy and paleoenvironmental reconstruction. *Palaeoworld* **15**, 217–222 (2006).

40. Li, G. *et al.* Early Cambrian metazoan fossil record of South China: Generic diversity and radiation patterns. *Palaeogeogr. Palaeoclimatol. Palaeoecol.* **254**, 229–249 (2007).

41. Wang, D. *et al.* Coupling of ocean redox and animal evolution during the Ediacaran-Cambrian transition. *Nat. Commun.* **9**, 2575 (2018).